IEEE Access
Multidisciplinary ⋮ Rapid Review ⋮ Open Access Journal

Received 10 September 2022, accepted 16 September 2022, date of publication 27 September 2022,
date of current version 30 September 2022.

Digital Object Identifier 10.1109/ACCESS.2022.3208109

RESEARCH ARTICLE

Soil Moisture Monitoring Through UAS-Assisted Internet of Things LoRaWAN Wireless Underground Sensors

FAHIM FERDOUS HOSSAIN[1], RUSS MESSENGER[1], GEORGE L. CAPTAIN[1], SABIT EKIN[1], (Senior Member, IEEE), JAMEY D. JACOB[2], SALEH TAGHVAEIAN[3], AND JOHN F. O'HARA[1], (Senior Member, IEEE)

[1]School of Electrical and Computer Engineering, Oklahoma State University, Stillwater, OK 74078, USA
[2]School of Mechanical and Aerospace Engineering, Oklahoma State University, Stillwater, OK 74078, USA
[3]Biological Systems Engineering, University of Nebraska-Lincoln, Lincoln, NE 68588, USA

Corresponding author: John F. O'Hara (oharaj@okstate.edu)

This work was supported in part by the United States Geologic Survey (USGS) under Award G16AP00077, in part by the National Science Foundation (NSF-EPSCoR) under Award OIA-1946093, and in part by the OSU Unmanned Systems Research Institute.

ABSTRACT With growing usage and demand for the global freshwater supply, there is an increasing need for technologies that facilitate water conservation and environmental stewardship in irrigated agriculture. Toward this end, recent demonstrations of Internet of Things (IoT) sensors have revealed the value of wireless soil moisture content sensors. However, existing wireless solutions often employ above-ground wireless communication modules that physically interfere with routine farming operations. Underground wireless network solutions are severely challenged by the large radio-frequency (RF) propagation loss through soil. This paper presents a method that overcomes both problems by employing completely buried underground IoT sensors and communication modules with UAS (uncrewed aircraft system) mounted LoRaWAN gateways. The UAS mounted LoRaWAN gateway eliminates the need for any in-field base stations and also allows the LoRa enabled sensors to transmit data over short distances with very low energy. Field tests were carried out using this approach to serve as a proof of concept. The RSSI (received signal strength indicator) demonstrates that the proposed solution has good communication link margin and a significantly larger communication range than is necessary for reliable operation. Moreover, this solution is easy to build, scalable, cost-effective, and can be implemented in a highly power efficient fashion.

INDEX TERMS Internet of Things (IoT), long range radio (LoRa), scientific irrigation scheduling, soil moisture monitoring, uncrewed aircraft system (UAS).

I. INTRODUCTION

The growing worldwide population presents an increasing impetus to properly manage the sources and strains on the global freshwater supply. Agriculture is the biggest consumer of global freshwater supply while about half of the world population experiences water scarcity [1]. Nevertheless, maintaining some minimum required soil moisture is important in various biophysical processes like plant growth, germination of seeds, nutrient cycling and sustenance of the natural biodiversity in soil [1]. On the other hand, over-irrigation can be equally destructive, causing salinization [2] of the land and pollution [3] of freshwater sources when chemigated water is used for irrigation. The objective then becomes to always provide the optimal level of irrigation, just enough to maintain required soil moisture level. This is referred to as scientific irrigation scheduling [4] which falls under the umbrella of precision agriculture, and soil moisture monitoring is an important element in meeting this objective [5], [6].

There are different ways of sensing and monitoring soil moisture levels in agricultural fields. Generally, crop fields have large areas, therefore implementing a wireless solution

The associate editor coordinating the review of this manuscript and approving it for publication was Ghufran Ahmed.

for monitoring soil moisture is preferable to avoid the cost and complexity of laying and maintaining long lengths of cable. In the wireless scheme, multiple sensors can be deployed in a field to set up a wireless sensor network that can convey soil moisture data from various parts of the field to the network server. Several wireless technologies have been demonstrated in this regard for precision agriculture, including GPRS (General Packet Radio Service), GSM (Global System for Mobile Communication), Wi-Fi, Bluetooth, and Zigbee [7]. In a similar application, forest fire monitoring systems based on Zigbee wireless sensors have also been demonstrated [8].

The research challenges of wireless underground sensor networks have been reviewed in [9]. If all sensor nodes and communication modules can be placed completely underground, then devices can avoid interfering with farm machinery, a significant attraction. The main challenge of this scheme is the high RF (radio frequency) path loss, which causes low data rate for a given power, or high power consumption for a given data rate compared to above-ground communication [9]. Data cannot be transported over long distance in an underground sensor network without excessive power use, so it must be re-routed relatively quickly to an above-ground stationary or mobile base stations or gateways [9]. This challenge is compensated by setting up a dense array of above-ground base stations, which is neither cost-effective nor practical. As a less traditional wireless solution, magnetic induction was also investigated for underground communication [10]. This technique leverages the lower material losses of non-propagating magnetic fields for communication, but also suffers a very short range due to the more rapid roll-off of near-field power density. Underground magnetic induction *waveguide* systems were subsequently investigated, which proved that a large range can be achieved by employing a large number of relay coils in short intervals between the transmitter and receiver [11]. While feasible, this dramatically increases the complexity and cost of this solution.

More possible agricultural solutions have emerged under the umbrella of the Internet of Things (IoT) - a vast network of relatively simple devices such as sensors and cameras, connected to the internet via (predominantly) wireless communication networks [12]. For example, [13] employed an IoT-based wireless sensor network to develop a Greenhouse Irrigation Management System to monitor various agricultural parameters including soil moisture. It is significant to this work that a variant of IoT called the Internet of Underground Things (IoUT) has developed with applications in agriculture wherein interconnected things are partially or completely placed underground [14].

LoRa is a wireless radio technology and LoRaWAN is a wide area network protocol that incorporates the LoRa technology [15]. In IoT applications, the LoRaWAN (Low Range Wide Area Network), or just LoRa, protocol has emerged as a very promising technology since it allows long range, low data rate wireless communication utilizing very low power LoRa enabled sensors [16]. After analyzing many different technologies, some researchers have concluded that for smart agricultural applications, LoRa is the best option [17]. LoRa uses chirped spread-spectrum modulation, with 433 MHz, 868 MHz, or 915 MHz as the carrier frequency – depending on region – with a maximum data rate of 50 kbps [18], which is more than adequate for soil moisture monitoring and occasional reporting. The relatively low carrier frequencies translate to manageable free-space path loss and some immunity to line-of-sight issues. This generally gives LoRa a coverage radius of between 1 to 10 km above ground. In a work published by Renzone *et al.* [19], LoRaWAN sensors were buried underground with different soil types and depths between 10 and 50 cm. In their experiment, they measured the corresponding path and packet loss using a receiver with its antenna placed on the ground 15 m horizontally away from the buried sensor. Additionally, in [19], the RSSI was measured over a 20 day time period to measure the impacts of soil compaction.

Another research avenue of environmental and agricultural monitoring involves uncrewed aircraft systems (UASs) [20]. The applications of UAS in the field of irrigation management have been comprehensively reviewed in [21]. UAS-based, low-altitude remote sensing technologies and wireless sensor networks have been studied for precision weed management [22] and for preventing frost in fragmented vineyards by monitoring temperature and humidity [23]. Soil moisture content monitoring using UAS-based hyperspectral imagery has also been demonstrated [24]. Ground sensor communication with UAS-based small cell networks was developed in [25]. The ground sensors have low energy and low coverage area while the UAS-SC (UAS-Small Cell) acts as a mobile transceiver that collects the data from the ground sensors by flying over them [25]. In this way a UAS can be used as a mobile gateway for low power IoT sensors. But in [25], above-ground communication modules were employed along with solar cells for powering the modules and sensors. These pose a significant practical hindrance for farm machinery operations.

In this paper, we present a soil moisture monitoring system which employs completely buried IoT sensors with integrated communication modules, no in-field base stations or gateways, and a UAS-based mobile gateway for retrieving the soil moisture data from the buried sensors. The buried sensors and the gateway aboard the UAS use LoRa-based wireless communication. A similar work [26] has been published by Cariou *et al.*; however, there are some important differences between our work and [26]. The operating frequency in our work is 916 MHz whereas in [26], the operating frequency is 868 MHz. Our sensor node was buried at a depth of 0.3 meters whereas the sensor node in [26] was buried at a depth of 0.15 meters. Generally, sensor nodes buried deeper into the ground can prove more beneficial as they are more likely to be cleared from farming machinery operations. In our work, from experimental data and path loss analysis, we have demonstrated that the relative antenna orientation of the buried sensor and the above ground gateway has little significance in communicating data packets - which in [26]

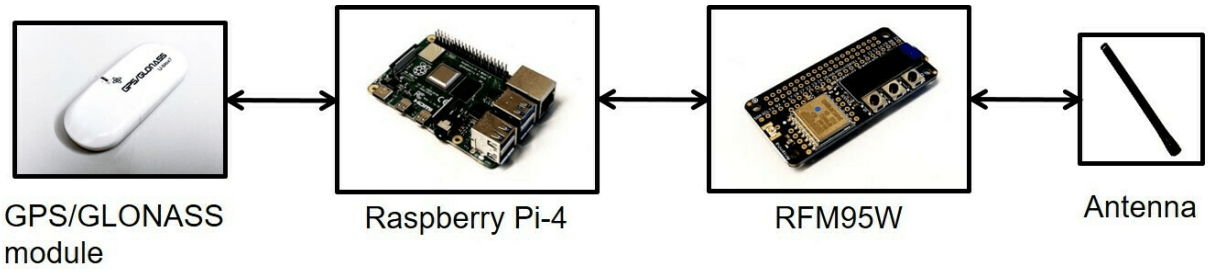

FIGURE 1. Block diagram for the mobile LoRaWAN gateway hardware (arrows indicate direction of data flow).

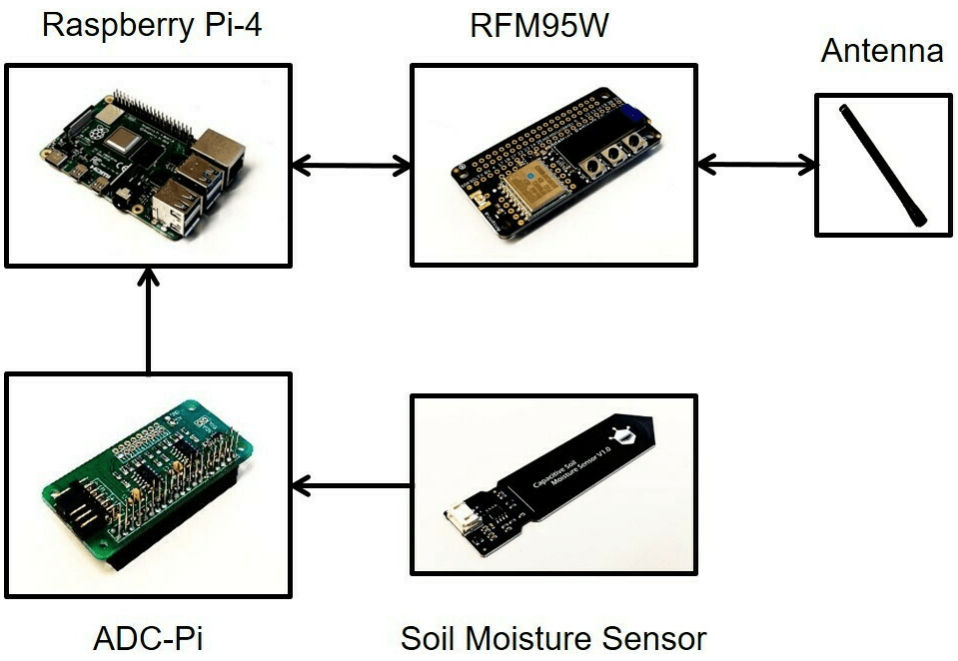

FIGURE 2. Block diagram for buried LoRa enabled sensor hardware setup (arrows indicate direction of data flow).

has not been presented. We have also presented our analysis of percentage packet loss with varying distances which in [26] has been mentioned to be done in future work. In [26], it has been shown that the RSSI (received signal strength indicator) values after a particular horizontal distance is higher at a higher altitude - the impact of the soil on the propagation of the signal has been attributed as the reason for this - whereas we have elaborated on the mechanisms of signal propagation from soil to air from an electromagnetic perspective and also using an electromagnetic simulation. In addition, unlike in [26], we have presented a plausible estimation of the battery lifetime of the LoRa enabled sensor node. The advantages of our proposed solution are threefold: First, since all the end node devices are buried completely underground, they do not interfere with normal farming operations; Second, since the UAS moves from one sensor to another to collect data, the sensor nodes can transmit very little energy, which makes them highly energy efficient and reduces the need for costly or frequent battery maintenance; Third, this solution is relatively simple and inexpensive to implement and scale. Based on experimental measurements, we quantitatively present the relevant channel qualities, network performance, and estimates of real-world limitations in terms of battery life and operational ranges.

II. MATERIALS AND METHODS

A. DEVELOPMENT of LoRaWAN GATEWAY and LoRa ENABLED SENSOR

1) MOBILE LoRaWAN GATEWAY HARDWARE

The LoRaWAN gateway used to collect data from the LoRa enabled sensor was primarily based on a Raspberry Pi 4. A LoRa module was added to function as the communication module along with a dipole antenna. When mounted on a UAS, the Raspberry Pi was also accompanied by a GPS/GLONASS (Global Positioning System/ Global Navigation Satellite System) module. The reason for using a GPS/GLONASS module will be apparent in a later section. The Raspberry Pi contained the programs necessary to control the LoRa module to collect data packets sent from the LoRa enabled sensor and it also acted as storage for the collected data. The Raspbian operating system was used to govern operations. A block diagram of the LoRaWAN gateway is shown in Fig. 1.

The LoRa radio was a bonnet-style RFM95W radio from Adafruit and plugged into the general purpose input/output (GPIO) pins of the Raspberry Pi. Depending on environmental obstructions, antenna type, frequency and power output, the range can approach approximately 2 km. For our purpose, a half-wave dipole antenna having a center frequency of 916 MHz was employed. It had a torus-shaped antenna pattern with 6 dBi of gain, and its bandwidth covered the entire ISM 900 MHz band. The 120 mm (4.72 inch) long antenna is rugged and damage-resistant and occupies little space.

2) LoRa ENABLED SENSOR HARDWARE

The LoRa enabled sensor or end node that was buried during the experiment also had a Raspberry Pi 4 as its controller, although a much simpler controller could be employed. A block diagram of the LoRa enabled sensor is shown in Fig. 2. Just like the mobile LoRaWAN gateway, an RFM95W LoRa radio module was plugged to the LoRa enabled sensor's Raspberry Pi 4 to enable sending data packets to the mobile LoRaWAN gateway. The radio can output between +5 dBm and +23 dBm power, which is configurable from software. A half-wave dipole antenna (center frequency 916 MHz) was connected to the RFM95W module. The radio was configured to operate with a 125 kHz bandwidth. A spreading factor (SF) of 7 and a coding rate (CD) of 5 were chosen for the RFM95W LoRa module - the same values were chosen for the gateway LoRa module. A capacitive soil-moisture sensor manufactured by DFRobot (model SEN0193) was used to measure the moisture of the soil.

The capacitive soil-moisture sensor produces an analog voltage between 0 to 3.3 volts depending on the moisture content of the soil. The analog output of the sensor was converted to digital bits via an analog to digital converter (ADC-Pi, PIS-1352) that was then fed into the Raspberry Pi. The ADC-Pi is a 17-bit ADC with eight channels for inputs. It can be configured to work at different data rates such as 3.75 Sa/s (samples per second) at 17-bits resolution, 15 Sa/s at 15-bits, 60 Sa/s at 13-bits, or 240 Sa/s at 11-bits. The ADC-Pi has two MCP3424 Microchip converters each having four analog inputs. The ADC-Pi communicates with the host Raspberry Pi via I^2C port and is powered by the GPIO port. The data rate, resolution, and gain of the ADC-Pi can be selected or changed within software. For our purposes, we configured the ADC-Pi to operate at a sample rate of 15 samples per second.

B. PRELIMINARY MEASUREMENTS

A plastic, water-tight enclosure was used to house the entire LoRa enabled sensor except for the soil moisture sensor, which was wired externally through a sealed gland so that it could be inserted into the soil. The antenna inside the enclosure was aligned on its linear axis in a north-south and horizontal orientation. An approximately 35 cm deep hole was dug and the LoRa enabled sensor was placed therein with the soil moisture sensor inserted horizontally into the unperturbed sidewall of the hole at a depth of approximately 30.5 cm. The hole was filled with soil so that the LoRa enabled sensor and broadcasting antenna were under 30.5 cm (1 foot) of soil. The LoRa enabled sensor was powered from a car battery, whose 12 V_{DC} supply was converted into 5 V_{DC} supply by a common USB charging pod. The DC power wires were run through the soil from the battery and voltage converter above the ground to the LoRa enabled sensor underground.

FIGURE 3. Data being recorded in preliminary experiment.

The portable LoRaWAN gateway was fixed at the end of a wooden pole with the antenna having the same orientation (co-polarized) as the LoRa enabled sensor's antenna. The LoRaWAN gateway was powered by a small, portable battery. Data sent from the buried sensor were received by the LoRaWAN gateway and the received signal strength indicators (RSSI) were logged as a function of several LoRaWAN gateway positions relative to the end-node, both at different distances and heights. Numerous distances were selected in both the south and west directions, all at several heights. In addition, to get an estimate of the maximum coverage area of the buried LoRa enabled sensor, single-point measurements were collected when the LoRaWAN gateway was moved as far as possible to the north, south, east, and west directions until the data packets were no longer received. All the same measurements were repeated after changing the orientation of the LoRaWAN gateway antenna to east-west, which put the transmit and receive antennas in a cross-polarized relative orientation. Fig. 3 shows an image of the research team collecting data during the preliminary experiment.

C. UAS-BASED MEASUREMENTS

After the preliminary experiment, the LoRaWAN gateway was mounted on a UAS. The UAS employed was the DJI Phantom 4 Pro. This UAS has a maximum battery lifetime of approximately 30 minutes, a top speed of 72 kph, and a

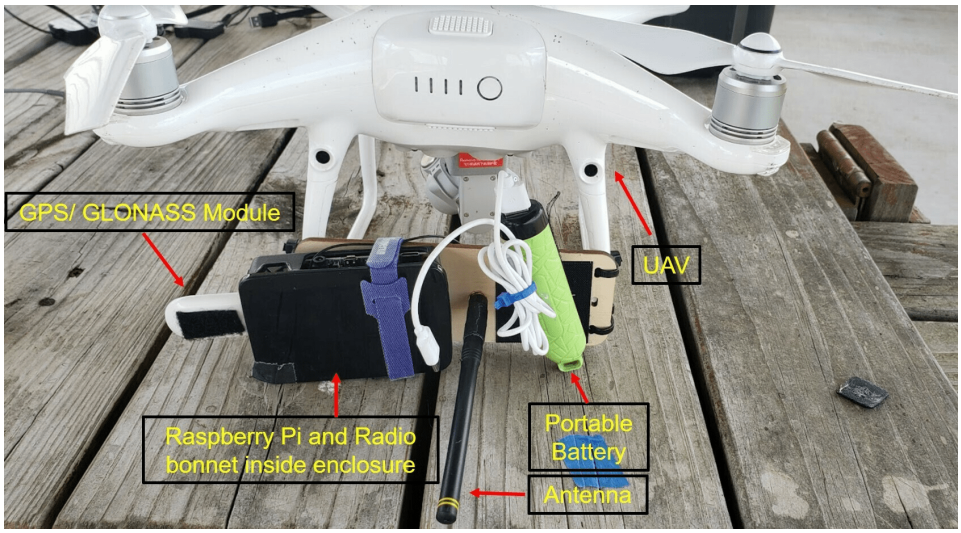

FIGURE 4. LoRaWAN gateway mounted on UAS.

weight of 1,388 g. The UAS has an onboard GPS/GLONASS module with an accuracy of ±0.5 m vertically and ±1.5 m horizontally. As before, the LoRaWAN gateway consisted of a Raspberry Pi, a portable battery, a separate GPS/GLONASS module, and the antenna mounted to the front side of the UAS. The UAS hardware setup is shown in Fig. 4. The two GPS/GLONASS modules were used to synchronize data between the UAS and LoRaWAN gateway. The UAS provided flight logs with accurate position data and timestamps. The LoRaWAN gateway was programmed to synchronize the time with GPS time. Once synchronized with GPS time, the data received from the buried sensor's transmitter was timestamped with the LoRaWAN gateway's time. When processing the data, the LoRaWAN gateway timestamps were matched to the UAS timestamps so that RSSI data from the LoRaWAN gateway could be accurately matched with corresponding position data from the UAS's flight log. The flight path of this system was uploaded to the UAS via Litchi [27] and resembled a grid of points in an outward spiral. This grid was approximately 46 m × 46 m (150 ft × 150 ft) and the UAS was flown at 0.91 m (3 ft) intervals from 0.91 m to 3.66 m (12 ft) height. All UAS-based measurements were performed with the LoRaWAN gateway antenna in co- and cross-polarized orientations. Litchi allows the user to upload a CSV file of points to define a flight path. A Python script was written to generate the coordinates at each height and save them to individual files. A Google-Earth view of the flight path of the UAS is shown in Fig. 5.

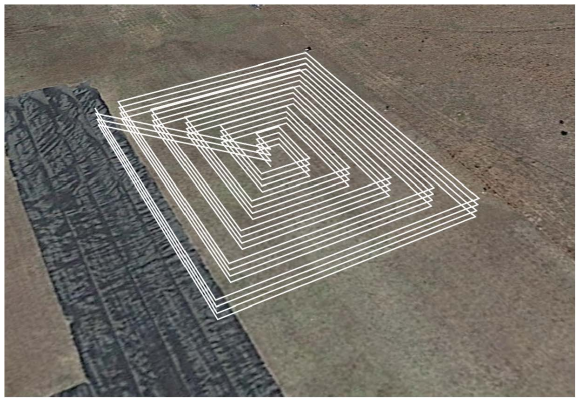

FIGURE 5. Spiral flight path of the UAS viewed via Google Earth. Data collection at each flight level began at the center of the spiral and proceeded outward.

III. RESULTS AND DISCUSSION

A. PRELIMINARY RESULTS

The received signal strength (RSSI) indicator data in dBm units were recorded during the preliminary measurement exercise. First the LoRaWAN gateway antenna orientation was co-polarized with the LoRa enabled sensor antenna while recording the RSSI data. Next, the LoRaWAN gateway antenna orientation was cross-polarized to the LoRa enabled sensor antenna orientation while measuring the RSSI data. The maximum usable distance – beyond which packet loss became 100% – was found to be greater than 36.5 m (120 feet).

Four heatmaps are shown in Fig. 6. Fig. 6(a) shows the RSSI values at different heights from ground and at different distances toward the west from the LoRa enabled sensor burial position. Fig. 6(b) shows the RSSI values at different heights from ground and at different distances towards the south from the LoRa enabled sensor burial position. Fig. 6(a) and Fig. 6(b) show that, at observation points not directly above the buried sensor, the RSSI value increases with increasing height. It is noted that the observation window is within 2 m height from ground surface and 5 m horizontal distance from the burial position of the sensor. However, when the LoRaWAN gateway antenna is directly above the LoRa enabled sensor antenna, the RSSI values decrease with increase in height. At a particular height, the RSSI values mostly decrease with increasing horizontal distance from the burial position of the LoRa enabled sensor. The mechanisms behind this behavior are discussed in detail in the Comparison

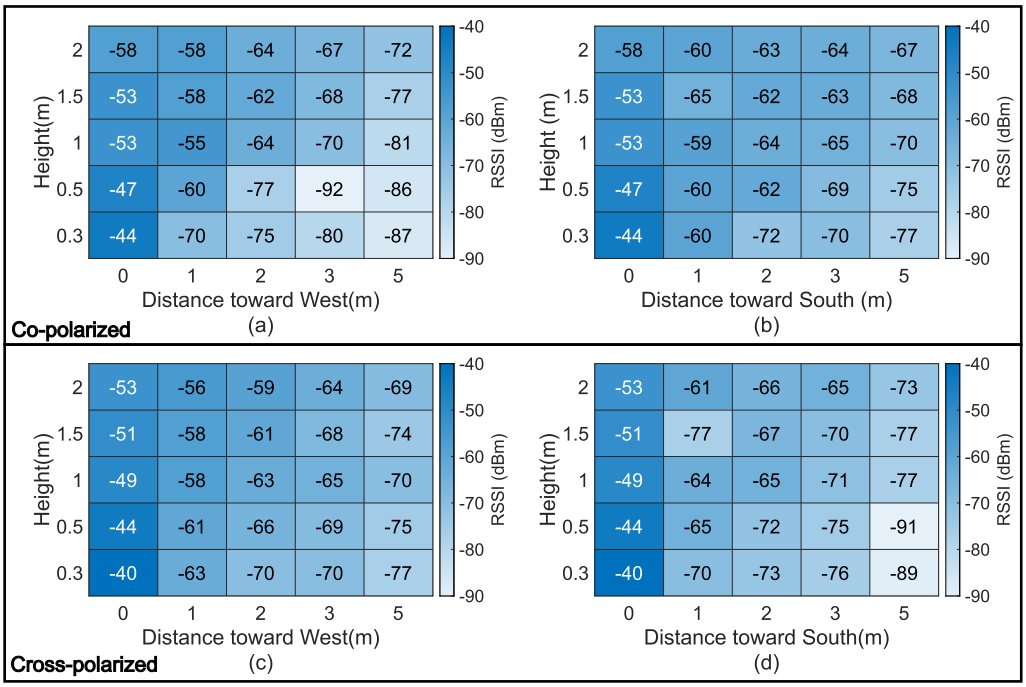

FIGURE 6. (a) and (b) RSSI in dBm when both LoRaWAN gateway and LoRa enabled sensor antenna are co-polarized. (c) and (d) RSSI in dBm when both LoRaWAN gateway and LoRa enabled sensor antenna are cross-polarized.

with Numerical Simulation section. In short, however, the radiation pattern of the buried dipole near the air-soil interface appears to be the principal factor in this observed behavior. Interestingly, these observations hold true for the measurements when the antennas were cross-polarized to each other - the data are shown in Fig. 6(c) and Fig. 6(d). Surprisingly, stronger RSSIs were frequently observed in a cross-polarized configuration. This suggests some significant mechanism of polarization rotation or randomization by wave scattering. Wave scattering does not occur significantly above ground, so it further suggests that polarization randomization occurs from multiple scattering events either within the soil or with the electronics surrounding the buried sensor antenna (or both). In this case, the electronics packaging, soil composition, soil compaction, and soil saturation would also likely affect the polarization state of the wave exiting the soil. Therefore, very careful measurements with tightly controlled soil parameters and system design would be required to isolate this mechanism, which is beyond the scope of this work.

B. DATA TAKEN FROM DRONE FLIGHT

When the LoRaWAN gateway was mounted on the UAS, the RSSI data were taken at heights of 0.91, 1.83, 2.74, and 3.66 meters (3, 6, 9, and 12 feet) over an area of approximately 2,090 m^2 (22,500 square feet). This data logging experiment was carried out two times. During the first time, the LoRaWAN gateway antenna and the LoRa enabled sensor antenna were co-linearly polarized and during the second time, the antennas were cross-polarized.

The LoRa enabled sensor's longitude and latitude were normalized to zero to present the measured data in Fig. 7(a) and Fig. 7(b). Here, it is observed that for a particular height, the RSSI values decrease with increasing distance from the LoRa enabled sensor's position. But, at a particular distance from the LoRa enabled sensor's position, the RSSI values generally increase with increase in height. However, directly above the LoRa enabled sensor, the increase in height accompanied reducing RSSI values. These results are congruent with the results of our preliminary measurement campaign.

C. PACKET LOSS ANALYSIS

The measurements were then analyzed in terms of packet loss. The LoRaWAN gateway encountered a best case packet loss of 12% when the antennas were co-polarized and 10% when the antennas were cross-polarized. Packet loss can also be quantified for different intervals of distances. Fig. 8(a) and Fig. 8(b) show the percentage packet loss computed for various intervals of distances between the UAS-mounted LoRaWAN gateway and the buried LoRa enabled sensor. Fig. 8(a) indicates that when the antennas were co-polarized, percentage packet loss was no more than 15% for distances smaller than 61 m and after this distance the percentage packet loss increases dramatically. From Fig. 8(b), it can be seen that when the antennas were cross-polarized, percentage packet loss was no more than 17% for distances smaller than 82 m. The horizontal distance is contributing the most to the packet loss, compared to the height component, since the UAS never reached a height greater than 12 ft (3.66 m) from the ground. Summarily, the LoRaWAN gateway and the buried device could communicate without experiencing more than 17% packet loss at distances $\leq$61 m from each other. This is more than adequate for the intended purpose.

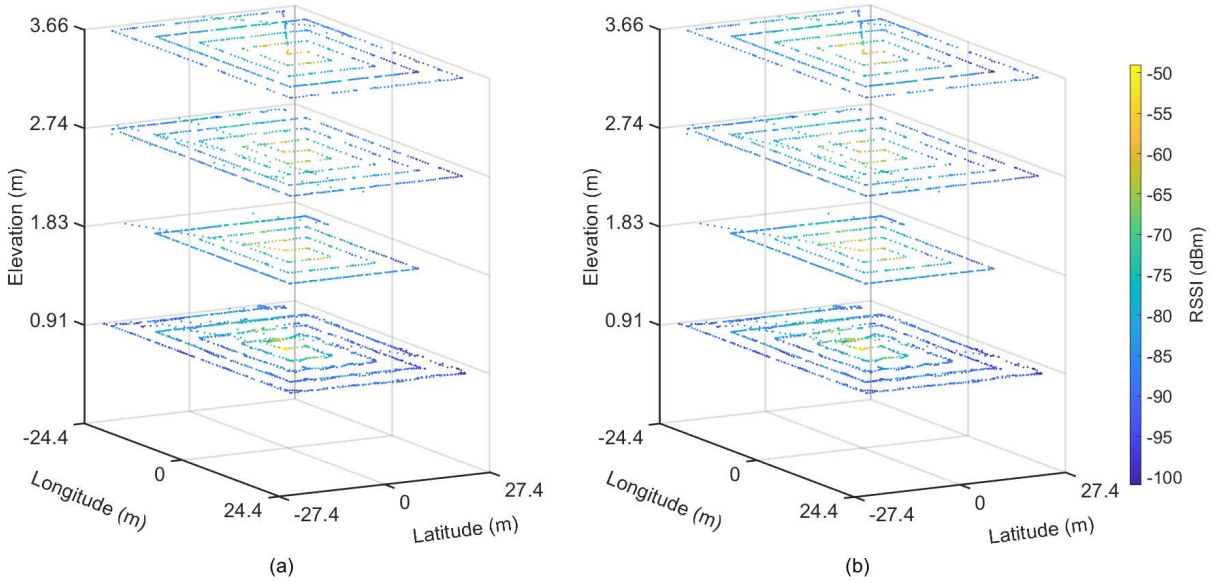

FIGURE 7. 3D heatmaps of RSSI in dBm when (a) both LoRaWAN gateway and LoRa enabled sensor antennas were co-polarized and (b) when the antennas were cross-polarized.

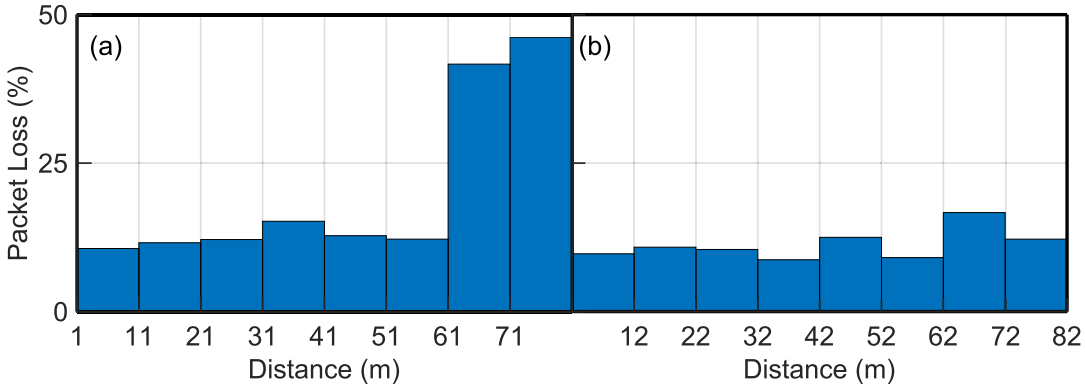

FIGURE 8. (a) Percentage packet loss in different intervals of distance between UAS and buried sensor when antennas were in co-polarized orientation and (b) cross-polarized orientation.

D. BATTERY LIFETIME ANALYSIS

Another important question is the battery lifetime of the buried LoRa enabled sensor. It could clearly be made more power efficient if a low-power microprocessor was employed instead of a Raspberry Pi. The Texas Instruments IC MSP430AFE2 $\times$ 3 is one example alternative. In principle, the microprocessor could normally be in low-power standby mode and only wake 24 times a day. Each awakening would last for about one second to collect data from the soil sensor and store it in memory. The one exception would be when it is also tasked with transmitting data to the LoRaWAN gateway. The soil sensor itself can also be powered for only one second, every time the microprocessor wakes up. In addition, the UAS can collect data from any one LoRa enabled sensor only once a day, at a scheduled time. In this scenario, each LoRa enabled sensor is awake for a total of less than 1 min per day.

For a more conservative estimate of battery life, we can assume the radio RFM95W is active in beacon mode during a five minute window every day for transmitting data. If the transmit time is set to 0.13 s and the idle time between each transmission is set to 4.7 s (typical values), then over the course of the five minute beacon mode, the total transmission time will be approximately 8.5 s. The current draw for each component device was obtained from their respective data sheets. Using these currents, the radio's delivered power (+20 dBm) to the antenna, and supply voltage (3.3 V), the average power draw by the LoRa enabled sensor can be estimated for both its active and dormant period. Under these conditions and assuming a battery total capacity of approximately 9,000 J and a 1.5 V to 3.3 V converter circuit efficiency of 80%, the LoRa enabled sensor should be able to operate without battery maintenance for about 3.5 years. It is noted that the duration the sensor node stays awake every time it wakes up and the number of times the sensor wakes up in a day can vary depending on the application, which will impact the battery lifetime. Moreover, the sensor nodes may be required to wake up at different times on different days to send their stored data to the UAS-mounted gateway. As an example, inclement weather may prohibit UAS flight on a particular day. Data storage with on-board sensor memory

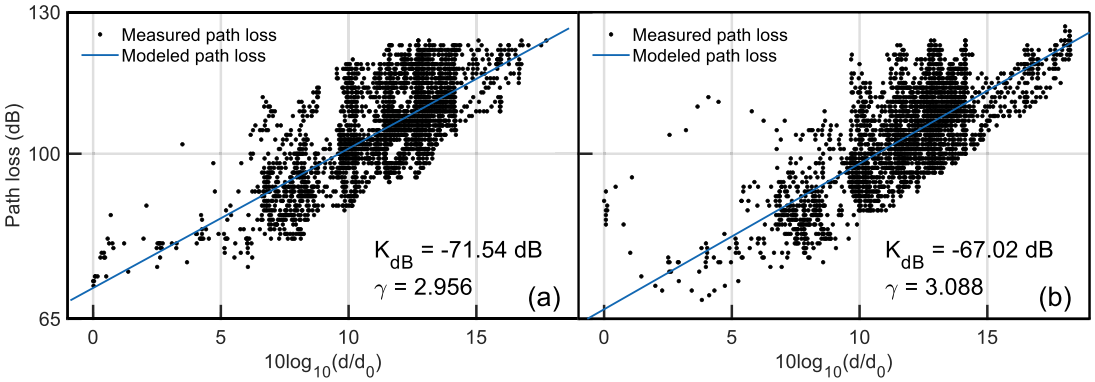

FIGURE 9. Measured and modeled path loss for the cases where the antennas are (a) co-polarized, (b) cross-polarized.

would usually permit this data to be collected later, but such considerations remain important in a system-wide design. In another application, the gateway could actively wake the sensor nodes when they reach close proximity. Reference [28] discusses methods of waking up sensor nodes by a gateway mounted on a UAS using radio frequency signals. Such variations on the communication scheme could easily change battery life estimates by significant amounts and must be considered for each particular application.

E. PATH LOSS ANALYSIS

The loss of signal strength of a wave traveling between the transmitter and receiver is quantified by the path loss. At a given distance d from the transmitter, the received signal power P_R can be written as follows [29]:

$$P_R = KP_T(d_0/d)^{\gamma} \tag{1}$$

where K is a dimensionless constant that is dependent on the transmission frequency and antenna characteristics, P_T is the transmitted power of the signal by the transmitter in watts, d_0 is a far-field (relative to the transmitter) reference distance in meters and γ is the dimensionless path loss exponent. K in dB can be expressed as

$$K_{dB} = 10\log_{10} K \tag{2}$$

The K_{dB} value signifies the minimum loss at reference distance. The path loss, P_{LdB} may then be quantified as

$$P_{LdB} = \gamma 10\log_{10}\left(\frac{d}{d_0}\right) - K_{dB}, \tag{3}$$

where $P_{LdB} = 10\log_{10}(P_T/P_R)$ is the path loss in decibels. In our case, $d_0 = 1.2192$ m, which is the minimum measured distance between the UAS and the buried sensor. Separate path loss analyses were done for the cases when the antennas were co-polarized and cross-polarized. The measured and modeled path losses versus distance are shown in Fig. 9(a) and Fig. 9(b). Using MATLAB's curve fitting tool, the path loss versus distance lines were fitted in the measured data. The curve fitting analysis shows that $K_{dB} = -71.54$ dB and $\gamma = 2.956$ for the co-polarized antenna case. When the antennas were cross-polarized, the values were $K_{dB} = -67.02$ dB and $\gamma = 3.088$. The high K_{dB} values can be attributed to the attenuation of the wave by the soil and the moisture in the soil. In the ideal case, $\gamma = 2$, which indicates a path loss exponent of free space. The fact that our values of γ are greater than two in both cases is a consequence of the transmitted signal partially traveling through soil and also experiencing the effects of the soil-air boundary, as described further below. The γ value in the case of cross-polarized antennas is larger than the co-polarized case which is expected. This means that for a real-world application, keeping the transmitter and receiver antenna in parallel will be statistically advantageous, although this benefit is surprisingly slight. In practice, the polarization state of the antennas would have little significant effect.

F. COMPARISON WITH NUMERICAL SIMULATION

A numerical simulation was performed in COMSOL Multiphysics to obtain the radiated power pattern of the buried antenna and thereby better understand the mechanisms limiting performance. The soil properties assumed in these simulations were comparable to those of the site of our preliminary measurements. To get these properties, we entered the coordinates of the site in the USDA Web Soil Survey website [30] and obtained an estimate of the soil composition. We also measured the volumetric water content of the soil on the site, which was found to be 41.4% at 12 inches depth into soil, obtained using a calibrated meter, Campbell Scientific Hydrosense II. Incidentally, this is quite wet and lossy soil, having just experienced rain in previous days. From these we obtained values of the complex relative electric permittivity as $\tilde{\epsilon}_r = 24.5 - j2.23$ (where $j = \sqrt{-1}$) by exploiting the empirical equations in [31]. The complex relative magnetic permeability was assumed to be unity. The complex permittivity and permeability were assumed to be frequency independent as our operating bandwidth was only 125 kHz. Consequently, the simulation was performed for only one frequency, i.e. 915 MHz. From the simulation, radiated power was examined in two vertical planes (both perpendicular to ground) - one plane is parallel to the antenna axis and contains the antenna axis center line while the other plane bisects the antenna and is perpendicular to its axis. In both cases, the

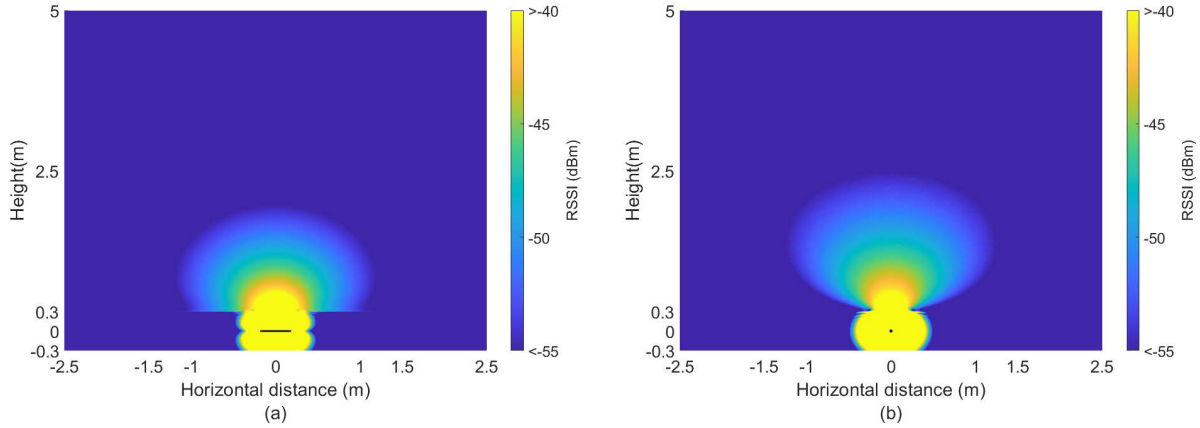

FIGURE 10. (a) Antenna power pattern for the vertical plane parallel to the antenna. The solid black line at a height of zero meters is the antenna. (b) Antenna power pattern for the vertical plane perpendicular to the antenna axis. The black dot at a height of zero meters is the antenna.

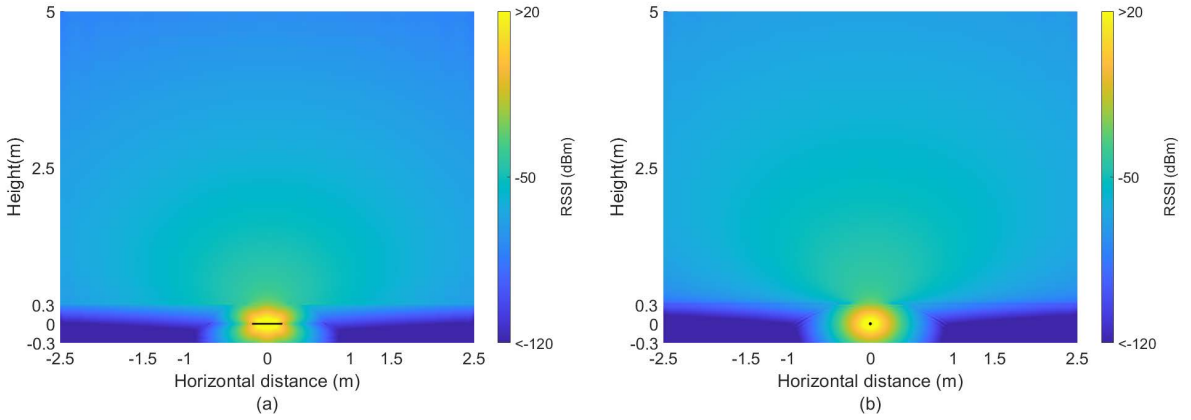

FIGURE 11. (a) Antenna power pattern for the vertical plane parallel to the antenna. The solid black line at a height of zero meters is the antenna. (b) Antenna power pattern for the vertical plane perpendicular to the antenna axis. The black dot at a height of zero meters is the antenna.

antenna is oriented parallel to the soil-air interface. The power patterns in the two planes are depicted in Fig. 10. In the figure, the antenna is at height of 0 m. It is surrounded by soil both above and below it for 0.3 m (1 ft), and at heights greater than 0.3 m the material is air. By looking at both patterns, it is apparent that the power is concentrated above and surrounding the antenna. As the horizontal distance and height from the antenna increase, the power decreases rapidly. This is particularly true in the soil where the high conductivity induces strong absorption losses that lead to simulated power values lower than -125 dBm within less than 1 m of propagation. This is shown more clearly in Fig. 11, which is the same data but with an increased color scale to clarify the behavior in the soil. There also appears to be significant reflection losses at the soil-air boundary which are highly exacerbated near or beyond the critical angle formed because of the smaller permittivity of air versus soil. Any plane wave incident upon the soil-air interface at an angle greater than critical angle (about 10.7° in this case) suffers complete reflection back into the soil. Nevertheless, there remains some signal coverage even just above the interface due to the strongly refracted waves. We point out that a strict plane wave interpretation of these phenomena is not possible due to the close proximity of the antenna to the interface. It is worth mentioning that the simulated power pattern inside the soil just next to the antenna is dominated by near field components, which would normally die off and become insignificant in the far-field (air). The near field components can act as energy storage (resonant) fields which leads to artificially inflated values of RSSI inside the soil next to the antenna using our simple power calculation method ($P \propto |\mathrm{E}|^2$).

In addition, Figs. 10 and 11 show that the power pattern within the soil looks similar to that of a $\lambda/2$ dipole antenna. On the other hand, it is reshaped in air by the discontinuity at the soil-air interface. Of particular note is that the critical angle interface produces strongly refracted waves that propagate parallel to the interface on the air side (see Fig. 10(a)). This represents power flow in directions that would be forbidden from an unbounded dipole antenna (parallel to the antenna axis), which is possibly another benefit to this application.

Simulation further permits a one-to-one comparison of power flow results with the experimental results obtained in preliminary measurements. These corresponding power patterns are compared in Fig. 12.

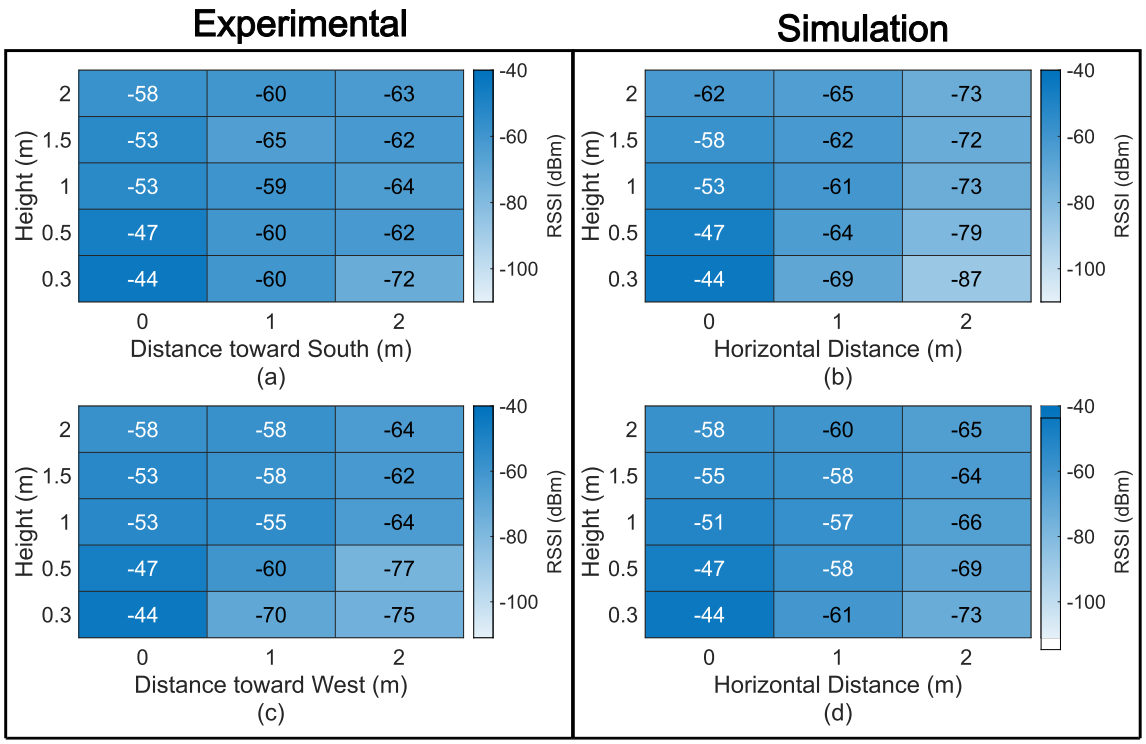

FIGURE 12. Comparison of (normalized) simulations and measured RSSI values from preliminary measurements. Only the case of co-polarized antennas is shown. (a) Antenna power pattern from preliminary experimental data for the vertical plane parallel to the antenna; (b) antenna power pattern from simulation for the vertical plane parallel to the antenna. (c) Antenna power pattern from preliminary experimental data for the vertical plane perpendicular to the antenna; (d) antenna power pattern from simulation for the vertical plane perpendicular to the antenna. All heights are measured from ground level and the antenna center is at the horizontal zero position.

In Fig. 12, each simulated power pattern is normalized to the maximum RSSI value obtained during preliminary measurements and then expressed in dBm. In both simulated cases (Fig. 12), the power values are calculated using only the electric field component that is parallel to the antenna. Looking at the power patterns in Fig. 12, it is seen that the patterns are similar in the sense that all of them have high power straight above the antenna and with the increase in height and horizontal distance from the antenna the observed power decreases.

Similar comparisons can be made for the case of cross-polarized antennas. But simulation results from COMSOL for cross-polarized orientation of antennas were on average 45 dB lower than that of co-polarized antenna simulations, which is to be expected due to the absence in simulation of any real-world perturbations to the wave polarization. Since the cross-polarized simulation results would imply undetectable signal levels, in contrast to measurements, there is no significant value to presenting this comparison. It is notable, however, that the experimental results proved the system more robust than expectations derived from simulation. In many cases, the measured RSSI was actually stronger than expected.

The similarity of the general trend in simulated power patterns and experimental power patterns in Fig. 12 suggests that the experimental power patterns were the result of various mechanisms including wave reflections from soil-air interface, complete reflection beyond critical angle, and large soil losses. A perfect match between simulated and measured power is certainly not expected. Some of the possible sources of error include the following. First, in the experiment the buried antenna was not immediately surrounded by soil; rather it was inside an air-filled (albeit small) plastic enclosure. Second, the buried antenna was placed next to other electronics including a Raspberry Pi and ADC which may have affected the radiation behavior. Finally, there may have been air pockets present in the soil above the buried enclosure containing the LoRa enabled sensor, an unavoidable result of perturbing the soil during digging and burying.

IV. CONCLUSION

The concept and experimental verification of using a UAS mounted LoRaWAN gateway with completely buried LoRa enabled sensors for soil monitoring is presented. Both manual and automated field measurements using a UAS revealed highly reliable communications over large distances (>36.5 meters), even with wet, lossy soil. Communication was found to be largely insensitive to antenna polarizations as evidenced by total packet losses of no more than 12%, regardless of antenna orientations. Having measured multiple heights, these tests also prove that this concept is viable even when the UAS needs to clear the heights of almost all kinds of crops. The simulations revealed that the signal crosses the soil-air boundary in a relatively narrow region

directly above the antenna, but this does not dramatically reduce the viability of the approach, since waves can refract sharply to the horizontal at the soil/air interface. Practically, the narrow emission region is irrelevant when the LoRaWAN gateway can hover directly above the LoRa enabled sensors. In addition, since LoRa enabled sensors can be buried at least 0.3 meters (1 ft) underground, they are very unlikely to interfere with normal farming operations. Finally, the measurements strongly suggest that LoRa enabled sensors can be developed with battery lifetimes on the order of multiple years, eliminating the need for regular maintenance. One disadvantage of this approach may be that a person may have to supervise the UAS flights. Although, if the UAS is programmed to be autonomous, then this approach can be utilized with minimal human intervention.

V. FUTURE WORK

In this work, one underground sensor node has been demonstrated to work in conjunction with a UAS mounted gateway. In future, the performance of this approach can be evaluated when multiple underground sensor nodes are deployed in a field. To collect the data from the underground nodes efficiently, the UAS may have to fly in a path that is energy efficient and fast - to this end, optimization algorithms can be exploited to optimize the flight path of the UAS. In addition, the performance of this approach can be investigated by burying the sensor nodes at different depths underground. Further refinements could also improve the simulations by including inconsistencies in the soil and including the surrounding electronics, e.g., the Raspberry Pi and its housing.

ACKNOWLEDGMENT

The authors thank Taylor Mitchell, Allan Burba, and Andrew Cole for their assistance with the UAS-based measurement campaigns.

REFERENCES

[1] B. Kashyap and R. Kumar, "Sensing methodologies in agriculture for soil moisture and nutrient monitoring," *IEEE Access*, vol. 9, pp. 14095–14121, 2021.

[2] D. Suarez, "Soil salinization and management options for sustainable crop production," in *Handbook Plant Crop Stress*, M. Pessarakli, Ed., 3rd ed. Boca Raton, FL, USA: CRC Press, 2010, ch. 3, pp. 41–54.

[3] M. Anderson, "Chemigation," in *Central Plains Irrigation Short Course and Exposition Proceedings*. Fort Collins, CO, USA: Colorado State Univ. Libraries, Feb. 1997, pp. 53–55.

[4] S. Taghvaeian, A. A. Andales, L. N. Allen, I. Kisekka, S. A. O'Shaughnessy, D. O. Porter, R. Sui, S. Irmak, A. Fulton, and J. Aguilar, "Irrigation scheduling for agriculture in the United States: The progress made and the path forward," *Trans. ASABE*, vol. 63, no. 5, pp. 1603–1618, 2020.

[5] T. Lakhankar, N. Krakauer, and R. Khanbilvardi, "Applications of microwave remote sensing of soil moisture for agricultural applications," *Int. J. Terraspace Sci. Eng.*, vol. 2, no. 1, pp. 81–91, Jan. 2009.

[6] S. Rawal, "IoT based smart irrigation system," *Int. J. Comput. Appl.*, vol. 159, no. 8, pp. 7–11, Feb. 2017.

[7] D. Thakur, Y. Kumar, A. Kumar, and P. K. Singh, "Applicability of wireless sensor networks in precision agriculture: A review," *Wireless Pers. Commun.*, vol. 107, no. 1, pp. 471–512, Apr. 2019.

[8] J. Zhang, W. Li, and N. Han, "Forest fire detection system based on a ZigBee wireless sensor network," *Frontiers Forestry China*, vol. 3, no. 3, pp. 369–374, 2008.

[9] I. F. Akyildiz and E. P. Stuntebeck, "Wireless underground sensor networks: Research challenges," *Ad Hoc Netw.*, vol. 4, no. 6, pp. 669–686, Nov. 2006.

[10] N. Jack and K. Shenai, "Magnetic induction IC for wireless communication in RF-impenetrable media," in *Proc. IEEE Workshop Microelectron. Electron Devices (WMED)*, Apr. 2007, pp. 47–48.

[11] Z. Sun and I. F. Akyildiz, "Magnetic induction communications for wireless underground sensor networks," *IEEE Trans. Antennas Propag.*, vol. 58, no. 7, pp. 2426–2435, Jul. 2010.

[12] E. A. Abioye, M. S. Z. Abidin, M. S. A. Mahmud, S. Buyamin, M. K. I. AbdRahman, A. O. Otuoze, M. S. A. Ramli, and O. D. Ijike, "IoT-based monitoring and data-driven modelling of drip irrigation system for mustard leaf cultivation experiment," *Inf. Process. Agricult.*, vol. 8, no. 2, pp. 270–283, Jun. 2021.

[13] A. N. Harun, M. R. M. Kassim, I. Mat, and S. S. Ramli, "Precision irrigation using wireless sensor network," in *Proc. Int. Conf. Smart Sensors Appl. (ICSSA)*, May 2015, pp. 71–75.

[14] M. C. Vuran, A. Salam, R. Wong, and S. Irmak, "Internet of underground things: Sensing and communications on the field for precision agriculture," in *Proc. IEEE 4th World Forum Internet Things (WF-IoT)*, Feb. 2018, pp. 586–591.

[15] A. J. Wixted, P. Kinnaird, H. Larijani, A. Tait, A. Ahmadinia, and N. Strachan, "Evaluation of LoRa and LoRaWAN for wireless sensor networks," in *Proc. IEEE SENSORS*, Oct. 2016, pp. 1–3.

[16] J. de Carvalho Silva, J. J. Rodrigues, A. M. Alberti, P. Solic, and A. L. Aquino, "LoRaWAN—A low power WAN protocol for Internet of Things: A review and opportunities," in *Proc. 2nd Int. Multidisciplinary Conf. Comput. Energy Sci. (SpliTech)*, Jul. 2017, pp. 1–6.

[17] S. Subashini, R. Venkateswari, and P. Mathiyalagan, "A study on LoRaWAN for wireless sensor networks," in *Computing, Communication and Signal Processing*. Singapore: Springer, Sep. 2019, pp. 245–252.

[18] M. A. Ertürk, M. A. Aydin, M. T. Büyükakkaşlar, and H. Evirgen, "A survey on LoRaWAN architecture, protocol and technologies," *Future Internet*, vol. 11, no. 10, p. 216, Oct. 2019.

[19] G. Di Renzone, S. Parrino, G. Peruzzi, A. Pozzebon, and D. Bertoni, "LoRaWAN underground to aboveground data transmission performances for different soil compositions," *IEEE Trans. Instrum. Meas.*, vol. 70, pp. 1–13, 2021.

[20] D. Gao, Q. Sun, B. Hu, and S. Zhang, "A framework for agricultural pest and disease monitoring based on Internet-of-Things and unmanned aerial vehicles," *Sensors*, vol. 20, no. 5, p. 1487, 2020.

[21] J. L. Chavez, A. F. Torres-Rua, W. E. Woldt, H. Zhang, C. C. Robertson, G. W. Marek, D. Wang, D. M. Heeren, S. Taghvaeian, and C. M. Neale, "A decade of unmanned aerial systems in irrigated agriculture in the Western U.S.," *Appl. Eng. Agricult.*, vol. 36, no. 4, pp. 423–436, Jan. 2020.

[22] Y. Huang, K. N. Reddy, R. S. Fletcher, and D. Pennington, "UAV low-altitude remote sensing for precision weed management," *Weed Technol.*, vol. 32, no. 1, pp. 2–6, Feb. 2018.

[23] J. Valente, D. Sanz, A. Barrientos, J. del Cerro, Á. Ribeiro, and C. Rossi, "An air-ground wireless sensor network for crop monitoring," *Sensors*, vol. 11, no. 6, pp. 6088–6108, Jun. 2011.

[24] X. Ge, J. Wang, J. Ding, X. Cao, Z. Zhang, J. Liu, and X. Li, "Combining UAV-based hyperspectral imagery and machine learning algorithms for soil moisture content monitoring," *PeerJ*, vol. 7, p. e6926, May 2019.

[25] S. Duangsuwan, C. Teekapakvisit, and M. M. Maw, "Development of soil moisture monitoring by using IoT and UAV-SC for smart farming application," *Adv. Sci., Technol. Eng. Syst. J.*, vol. 5, no. 4, pp. 381–387, 2020.

[26] C. Cariou, L. Moiroux-Arvis, F. Pinet, and J.-P. Chanet, "Data collection from buried sensor nodes by means of an unmanned aerial vehicle," *Sensors*, vol. 22, no. 15, p. 5926, Aug. 2022.

[27] Litchi. (Apr. 2022). *Litchi for DJI Drones*. [Online]. Available: https://flylitchi.com/

[28] J. Chen, Z. Dai, and Z. Chen, "Development of radio-frequency sensor wake-up with unmanned aerial vehicles as an aerial gateway," *Sensors*, vol. 19, no. 5, p. 1047, Mar. 2019.

[29] A. Goldsmith, "Path loss and shadowing," in *Wireless Commun.*, 1st ed. New York, NY, USA: Cambridge Univ. Press, 2005, ch. 2, p. 46.

[30] United States Department of Agriculture. (2022). *Web Soil Survey*. [Online]. Available: https://websoilsurvey.sc.egov.usda.gov/

[31] N. R. Peplinski, F. T. Ulaby, and M. C. Dobson, "Dielectric properties of soils in the 0.3–1.3-GHz range," *IEEE Trans. Geosci. Remote Sens.*, vol. 33, no. 3, pp. 803–807, May 1995.

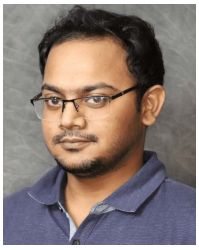

FAHIM FERDOUS HOSSAIN received the B.Sc. degree in electrical and electronic engineering from the Bangladesh University of Engineering and Technology, Dhaka, Bangladesh, in 2016. He is currently pursuing the Ph.D. degree with the Ultrafast Terahertz and Optoelectronics Laboratory, Oklahoma State University, Stillwater, OK, USA. He was a Lecturer at the Electrical and Electronic Engineering Department, Uttara University, Dhaka, from 2016 to 2017. His research interests include wireless communication, artificial electromagnetic materials, and terahertz measurement systems.

RUSS MESSENGER received the B.Sc. and M.S. degrees in electrical engineering from Oklahoma State University (OSU), Stillwater, OK, USA, in 2019 and 2021, respectively, where he is currently pursuing the Ph.D. degree in electrical engineering under his advisor Dr. John F. O'Hara. He is currently working as a Graduate Research Assistant with the Ultrafast Terahertz and Optoelectronic Laboratory, School of Electrical and Computer Engineering, OSU. His current research interests include the Internet of Things, intelligent reflecting surfaces, terahertz band wireless communication, and terahertz time domain spectroscopy.

GEORGE L. CAPTAIN is currently pursuing the bachelor's degree in electrical engineering and computer engineering with a minor in computer science with Oklahoma State University. He expects to graduate in the Fall Semester of 2022. He is currently an Undergraduate Research Assistant with the Ultrafast Terahertz Optoelectronics Laboratory. During the summer of 2021, he received the OK EPSCoR Research Experience for undergraduates grant to work on soil monitoring assisted by UAV.

SABIT EKIN (Senior Member, IEEE) received the B.Sc. degree in electrical and electronics engineering from Eskisehir Osmangazi University, Turkey, in 2006, the M.Sc. degree in electrical engineering from New Mexico Tech, Socorro, NM, USA, in 2008, and the Ph.D. degree in electrical and computer engineering from Texas A&M University, College Station, TX, USA, in 2012. He has four years of industrial experience as a Senior Modem Systems Engineer at Qualcomm Inc., where he has received numerous Qualstar Awards for his achievements/contributions on cellular modem receiver design. He is currently an Associate Professor of electrical and computer engineering at Oklahoma State University (OSU). He is also the Founding Director of the OSU Wireless Laboratory (OWL). His research interests include the design and analysis of wireless systems, including mmWave and terahertz communications in both theoretical and practical point of views, visible light sensing, communications and applications, non-contact health monitoring, and the Internet of Things applications.

JAMEY D. JACOB received the B.S. degree in aerospace engineering from the University of Oklahoma, in 1990, and the M.S. and Ph.D. degrees in mechanical engineering from the University of California at Berkeley, in 1992 and 1995, respectively. He is currently the Director of the OSU Unmanned Systems Research Institute and the John Hendrix Chair and a Professor of aerospace engineering with the School of Mechanical and Aerospace Engineering, Oklahoma State University. His current efforts are focused on advanced air mobility and their enhanced operation in the national airspace for broader innovative applications. He is currently lead on the NASA University Leadership Initiative Program WINDMAP to develop aviation weather solutions for advanced aerial mobility applications, including drones and urban air taxis, and the Director for the Counter-UAS Center of excellence. He was a National Research Council Summer Faculty Fellow at the Air Force Research Laboratory. He received the SAE Ralph Teetor Award, the Lockheed Martin Teaching Award, and the OSU Regents Distinguished Teaching and Research Awards, among other mentoring accolades. He is a native Oklahoman and dedicates much of his efforts to STEM workforce development, tribal engagement, and increasing diversity in engineering and science.

SALEH TAGHVAEIAN received the B.S. and M.Sc. degrees in irrigation engineering from the Ferdowsi University of Mashhad, Iran, in 2003 and 2006, respectively, and the Ph.D. degree in irrigation engineering from Utah State University, in 2011. He was a Postdoctoral Fellow at Colorado State University, from 2011 to 2013. He then joined the Biosystems and Agricultural Engineering Department, Oklahoma State University, as a State Water Resources Extension Specialist. In August 2022, he joined the Biological Systems Engineering Department, University of Nebraska, where he is currently serving as an Associate Professor. His research interests include sensor technologies for optimizing on-farm water management, irrigation scheduling, and crop water stress monitoring.

JOHN F. O'HARA (Senior Member, IEEE) received the B.S. degree in electrical engineering from the University of Michigan, in 1998, and the Ph.D. degree in electrical engineering from Oklahoma State University, in 2003. He was the Director of Central Intelligence Postdoctoral Fellow at Los Alamos National Laboratory (LANL) until 2006. From 2006 to 2011, he was with the Center for Integrated Nanotechnologies (LANL), and worked on numerous metamaterial projects involving dynamic control over chirality, resonance frequency, polarization, and modulation of terahertz waves. In 2011, he founded a Consulting/Research Company, Wavetech, LLC. In 2017, he joined Oklahoma State University, where he is currently an Assistant Professor and the Jack H. Graham Endowed Fellow of engineering. His research interests include metamaterials, terahertz communications, the Internet of Things applications, and photonic sensing technologies. He has around 100 publications in journals and conference proceedings.